Three-dimensional discrete element modelling of rubble masonry structures from dense point clouds

Nicko Kassotakis[1], Vasilis Sarhosis[2,*], Belen Riveiro[3], Borja Conde[3], Antonio Maria D'Altri[4], Jon Mills[1], Gabriele Milani[5], Stefano de Miranda[4], Giovanni Castellazzi[4]

[1]School of Engineering, Newcastle University, Newcastle upon Tyne, NE1 7RU, UK
[2]School of Civil Engineering, University of Leeds, Leeds, LS2 9JT, UK
[3]Department of Materials Engineering, Applied Mechanics and Construction, School of Industrial Engineering, University of Vigo, C.P., Vigo 36208, Spain
[4]Department of Civil, Chemical, Environmental, and Materials Engineering (DICAM), University of Bologna, Viale del Risorgimento 2, 40136 Bologna, Italy
[5]Department of Architecture, Built Environment and Construction Engineering (A.B.C.), Politecnico di Milano, Piazza Leonardo da Vinci 32, Milan 20133, Italy

Abstract

This paper presents a framework for the three-dimensional structural analysis of full scale, geometrically complex rubble masonry structures from point clouds generated from Structure-from-Motion photogrammetry or terrestrial laser scanning. According to the method, a point-based voxelization algorithm was adopted, whereby a dense point cloud was down-sampled into equidistant points, bypassing the need for conventional intensive processes, such as watertight mesh conversion, to obtain the geometric model of the rubble masonry for structural analysis. The geometry of the rubble masonry structure was represented by a sum of hexahedral rigid blocks (voxels). The proposed "*point cloud to structural analysis*" framework was implemented to assess the structural stability of the southwest leaning tower of Caerphilly Castle in Wales, UK. Simulations were performed with the three- dimensional computational software 3DEC, based on the Discrete Element Method (DEM) of analysis. Each voxel of the rubble masonry was represented as a rigid, distinct block while mortar joints were modelled as zero thickness interfaces which can open and close depending on the magnitude and direction of the stresses applied to them. The potential of the automated procedure herein proposed has been demonstrated to quantitatively assess the three-dimensional mechanical behaviour rubble masonry structures and provide valuable information to asset owners in relation to the structural health condition of assets in their care.

Keywords: Point cloud, rubble masonry, Discrete Element Method (DEM), terrestrial laser scanning, structure-from-motion photogrammetry

***Corresponding author:** Dr Vasilis Sarhosis, School of Civil Engineering, University of Leeds, Leeds, LS2 9JT, UK

Nomenclature

x_{min}	Minimum x-axis spatial coordinates	EVC	Empty voxelized point cloud
x_{max}	Maximum x-axis spatial coordinates	VAC	Volume adjustment coefficient
y_{min}	Minimum y-axis spatial coordinates	C	Joint cohesive strength
y_{max}	Maximum y-axis spatial coordinates	T	Joint tensile strength
z_{min}	Minimum z-axis spatial coordinates	φ	Joint friction angle
z_{max}	Maximum z-axis spatial coordinates	K_n	Joint normal stiffness
$Grid$	Voxel size	K_s	Joint shear stiffness

N_x	Number of voxels, x-axis	T_{max}	Maximum tensile force
N_y	Number of voxels, y-axis	F^s_{max}	Maximum shear force
N_z	Number of voxels, z-axis	A_c	Sub-contact area
Δ_x	Voxel dimension, x-axis	θ_t	Theoretical inclination angle
Δ_y	Voxel dimension, y-axis	g_h	Horizontal gravitational acceleration
Δ_z	Voxel dimension, z-axis	g	Vertical gravitational acceleration
P	Dense point cloud	λ_h	Horizontal inclination angle multiplier
P_x	Dense point cloud, x-axis	λ_v	Vertical inclination angle multiplier
P_y	Dense point cloud, y-axis	g_{hx}	Gravitational acceleration of, x-axis
P_z	Dense point cloud, z-axis	g_{hy}	Gravitational acceleration of, y-axis
Dim_x	Rounded point cloud x-axis	g_{vz}	Gravitational acceleration of, z-axis
Dim_y	Rounded point cloud y-axis	ψ	Azimuth of inclination
Dim_z	Rounded point cloud z-axis	$\lambda_{h,max}$	Critical inclination angle multiplier
Dim	Rounded point cloud	$U_{h,max}$	Critical horizontal displacement
DVC	Dimensionless voxelized point cloud		

1 Introduction

Despite advancements in computational mechanics and the substantial number of numerical techniques available, computational modelling of rubble historical masonry structures remains a complex task. This could be due to the anisotropic mechanical nature, lack of material characterisation and/or the complexity of geometry, which characterise many of these structures. Of the modern structural analysis tools available [1], the Discrete Element Method (DEM) has been demonstrated as highly effective in capturing the discrete nature of masonry structures subjected to quasi-static and dynamic loads [1-8]. For example, in [9], DEM models of rubble stone masonry walls with different section morphology have been developed to evaluate their out-of-plane structural capacity. Real masonry sections of walls surveyed from historical buildings were used. The geometries of the walls were generated using image-based computer-aided-design (CAD) files which were later imported in the discrete element model for their structural analysis. From the results, it was shown that the morphology of the stones in the wall significantly influences the stiffness and load-carrying capacity of the walls. However, the influence of the wall cross-section becomes more pronounced when assessing the displacement (the deformation capacity). Also, two dimensional (2D) numerical models based on the DEM were developed to study the structural stability of a historical rubble fortification [10]. The geometrical shapes used to represent the rubble masonry comprised of circular and polygonal elements randomly assembled. From this study, the suitability of the DEM for simulating the brittle behaviour of masonry and the need to accurately represent the geometric variability of the wall was also highlighted. In a further study, 2D models based on the DEM were used to investigate the out-of-plane capacity of rubble masonry walls with different cross-sections [11]. A drop in ultimate load-bearing capacity of rubble masonry walls with internal cavities and irregularly shaped blocks, as compared to panels of regular-shaped blocks, was found. From the above studies, it is evident that DEM is an effective modelling approach, able to account for the discrete and heterogeneous nature of masonry, yet detailed metrical geometric information is essential in order to perform accurate numerical analysis.

However, acquiring geometric features of rubble masonry using traditional manual surveying techniques and inputting them in a computational model for their structural analysis is a tedious process. With the development of remote sensing technology, such as terrestrial laser scanning (TLS) and Structure-from-Motion (SfM) photogrammetry, the metrical characteristics of irregular-shaped rubble masonry structures can be rapidly and reliably obtained [12]. Over the last decade, there has been some effort to capture geometrical characteristics from masonry structures and input them into numerical models for their structural analyses. For example, Riveiro et al. [13] used point clouds derived from TLS to develop a geometric model for the structural analysis of a stone masonry arch bridge (MAB) using thrust line analysis. The procedure involved manually converting raster images of the bridge into a geometric model. The same year, Lubowiecka et al. [14] generated a point cloud from a photogrammetric survey for the 3D documentation of a multi-span MAB. Subsequently, the geometric model developed was implemented into a 3D Finite Element Model (FEM) to assess the structural capacity of the arch. A methodology of automated point cloud segmentation of the arches, spandrels, and pavement was presented [15]. In [16], the same methodology was utilised to assess the structural capacity of a multi-span damaged historical MAB using geometric data from TLS and a structural analysis model based on the FEM.

Moreover, a method that automated the modelling of multi-story masonry building façades was developed by [17]. The procedure included the down-sampling of the original point cloud by means of voxelization and subsequent geometric model development. The investigation's main novelty lay in boundary feature detection. Thus, window and opening boundaries were detected by means of geometric criteria and implemented in a known-nearest-neighbours (KNN) algorithm. Geometrical validation of the proposed approached followed by comparing automatically developed models with manually developed CAD-based geometric models. The generated geometric models of the façades were analysed using commercial FEM software. The approach was later extended by using the so-called FacadeVoxel algorithm [18]. Also, a semi-automated numerical modelling methodology, named Cloud2FEM, was developed in [19] by applying a semi-automatic slicing algorithm to the point cloud. In this way, a geometric model was produced by joining each sliced segment and directly converting it into a finite element model avoiding any segmentation. This procedure has also been employed for the structural analysis of a historic masonry castle [20]. Moreover, within a general methodology employing automated 3D reconstruction for structural analysis, including the Cloud2FEM procedure also, the stability analysis of a leaning irregular tower has been performed in [21]. This was by means of automatically converting a point cloud generated from TLS into a triangulated mesh and then developing both FEM and Limit States models. The mechanical results between both applied methods showed good agreement. A non-uniform rational basis spline (NURBS) approach was followed and reported higher accuracy and flexibility compared to respective CAD geometric modelling. The geometric models were directly usable for FE analysis. What is more, structural analysis using FEM was performed by [22] to investigate the mechanical behaviour of a tower using models derived from point cloud data. Geometric model development was achieved by converting point clouds to meshes and using third-party software to convert the meshes into geometric models for subsequent FEM analysis. A "*Slicing Method*" was proposed in [23] which was used to convert the geometry of the façade into a structural analysis software based on FEM. A procedure for updating existing (CAD) geometric models with meshes from point clouds by means of computer vision algorithms was developed in [24]. Though this procedure was effective in adding details, it was not able to automatically develop geometric models; thus, not eliminating the need for initial CAD-based geometric model development. A methodology of automated FEM analysis from point clouds was developed in [25]. Point clouds were converted initially into triangular meshes and then into quad-meshes which were more manageable computationally and suitable for conversion into NURBS. The resulting geometric models were geometrically evaluated and found to be within 1 mm from the initial mesh.

From the above studies, whilst all these reported approaches provide an excellent platform for the structural analysis with the FEM using point cloud data, there are limited studies focusing on the automation of structural analysis of rubble masonry using DEM directly from point clouds. The aim of this paper is to present the development of an automated framework for the 3D discrete element modelling of rubble masonry directly from point clouds. The proposed framework implemented to assess the structural stability of the southwest leaning tower of Caerphilly Castle located in Wales, UK. The stability of the tower was structurally assessed using the discrete element method (DEM). Within DEM, the structure can be divided into an assemblage of discrete bodies that can move independently from each other. Also, within DEM, large rotations and displacements of blocks can be allowed and new contacts and loss of existing contacts between the elements are automatically recognised and updated as the calculation progresses. This paper is organized as follows: Section 2 describes the case study under consideration; Section 3 details the proposed "point cloud to structural analysis" framework; Section 4 presents the implementation of the proposed framework on the case study and the results obtained; and Section 5 outlines the conclusions and recommendations for future work.

2 The southwest leaning tower of Caerphilly Castle

The case study used to evaluate the proposed framework is the leaning tower of the Caerphilly tower located in South Wales, UK**Error! Reference source not found.**. Constructed in the 13th Century [26], Caerphilly is the second largest castle in the UK and one of the largest in Europe [27]. The southwest tower shown in Figure 1 is 17 m tall and 9 m in diameter [27]. It is reported to have been leaning for several centuries and stands at a current angle of approximately 10 degrees off vertical. The tower was constructed of rubble masonry, with a rough texture and indefinable joints. The most probable cause of leaning of the Caerphilly tower is attributed to the lack of foundation strength and stiffness which was induced by dewatering in the 18th Century.

Figure 1. Caerphilly Castle [27]. View of the face of the southeast leaning tower.

Over the last two decades, the numerical modelling of leaning towers has been investigated by many researchers [28-31]. There are also analytical approaches to investigate the safety of leaning towers. Notably, in [32], insight was provided into the critical inclination angle of leaning towers which were relied upon oversimplified material assumptions (rigid masonry without tensile strength and regular geometries). Such approaches cannot be applied to the present case study since the tower is highly irregular in shape, with openings, voids and a non-rectangular base. Recently, FEM and Limit Analysis have been successfully applied to perform structural analysis on leaning towers with complex geometry [20,21]. From such studies, it was shown that the FEM cannot always accurately describe the discontinuous nature of masonry [33], while Limit Analysis can, but still relies upon simplified assumptions and is not able to provide information about the in-service condition of the structure under consideration.

3 The proposed "point cloud to structural analysis" framework

In this section, the three-stage framework of the proposed automatic procedure for converting point clouds into 3D numerical models based on the DEM is described. The three-stage framework involved: Stage 1 - 3D documentation; Stage 2 - geometric model development; and Stage 3 -structural analysis. A flowchart of the proposed framework is shown in Figure 2 and a detailed description of the steps at each stage is provided below.

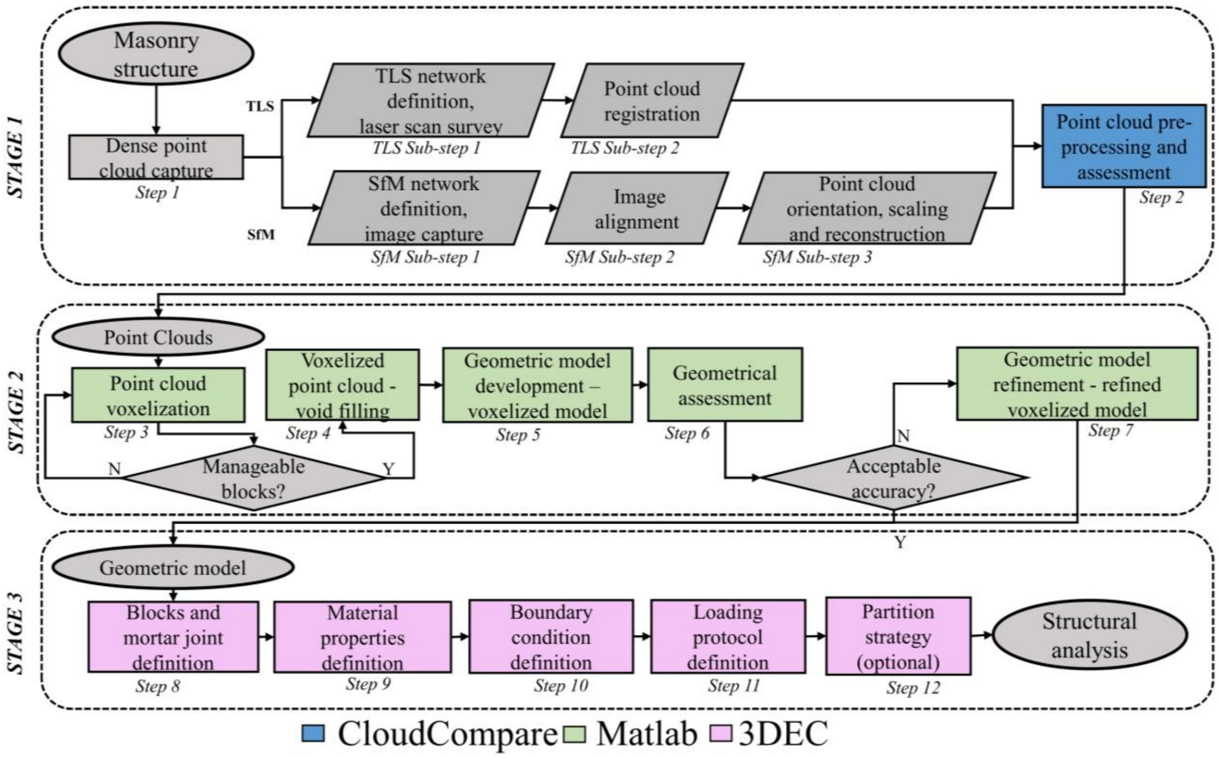

Figure 2. The "point cloud to structural analysis" framework.

3.1 3D Documentation – Stage 1

3.1.1 Step 1: Dense point cloud capture

The first step consists of capturing and processing the dense 3D point clouds from either an SfM photogrammetry or TLS campaign. The main processes of capturing photogrammetric point clouds are: (a) SfM photogrammetry network definition and image-capture; (b) image alignment and coarse reconstruction; and (c) orientation, scaling as well as dense reconstruction. The main processes involved in capturing TLS point clouds are: (a) TLS network definition and laser scan survey; and (b) scan registration. The term "*acceptable density*" refers to a density control after dense point cloud capture whereby the surface point spacing must be smaller than the required voxel grid size. If this is not the case, then voids will appear after voxelization. The completeness of the surface survey refers to achieving an accurate description of each portion of the structure. Multiple scan positions are suggested to ensure a full structure surface estimation. Figure 3**Error! Reference source not found.**a shows the dense point cloud obtained from a survey to document the structural health condition of the tower in 2014 [26]. In this instance, a FARO Focus 3D ×130 terrestrial laser scanner was used to acquire 27 scans of the entire castle. The main challenges related to the 3D documentation of the castle were the foreign objects (e.g. scaffolding, non-structural artefacts, and statues); and pedestrians since the site is a significant tourist attraction. Twelve spherical targets were used to complete the registration process for the entire survey.

3.1.2 Step 2: Point cloud pre-processing and assessment

A sampling procedure was first carried out to homogenise the spatial description of the point cloud. The density of the point cloud can be selected by the user, taking into consideration the architectural details of the structure. The choice of the point cloud density is important as it relates to the next step, namely the discretization by voxels. Typically, up-sampling of the point cloud is required for cases where the point cloud is poorly defined (e.g. roofs, openings, etc.). Cleaning and cropping of the point cloud were also carried out to remove noise and foreign objects/irrelevant points (e.g. non-structural elements such as vegetation, etc.) This is an important task since only the points relating to the structure being assessed should be considered in structural analysis. The open-source software CloudCompare [34] was used to clean and crop the point cloud. While cleaning and cropping, relative care was taken to retain the structure subject to structural analysis inside the point cloud, solely.

3.2 Geometric model development – Stage 2

3.2.1 Step 3: Point cloud voxelization

The developed voxelization algorithm herein presented was a point-based type, similar to the one proposed in [21] to [35]. It involved the down-sampling of the point cloud into a sum of equidistant points that had a common global axis orientation, as demonstrated in Figure 3b. The first process of point cloud voxelization consisted of the selection of the voxel size in meters (m), $Grid$. This voxel size defined the actual voxel dimension and appropriate choice for the correct accuracy and manageability of the structural analysis. The next process of voxelization consisted of finding the bounding box of the dense point cloud. The bounding box was composed of the minimum and maximum spatial coordinates (x_{max}, x_{min}), (y_{max}, y_{min}) and (z_{max}, z_{min}) of the dense point cloud, in meters. Then, the bounding box was subdivided into a grid with the user-defined voxel size equal to $Grid$ for the x, y, and z-axis respectively. The number of voxels for each axis (N_x, N_y, N_z) were defined by the following equations (1), (2) and (3). Ceil is the ceiling function used and $Grid$, the voxel size in meters:

$$N_x = \text{ceil}(\frac{(x_{max} - x_{min})}{Grid}) \quad (1)$$

$$N_y = \text{ceil}(\frac{(y_{max} - y_{min})}{Grid}) \quad (2)$$

$$N_z = \text{ceil}(\frac{(z_{max} - z_{min})}{Grid}) \quad (3)$$

The number of voxels is an integer due to the rounding of the ceiling function in equations (1), (2) and (3). This means that the voxel size and actual voxel dimensions cannot coincide. Thus, the actual voxel dimensions for the x, y and z axes were Δ_x, Δ_y and Δ_z respectively and defined by the equations (4), (5) and (6):

$$\Delta_x = \frac{(x_{max} - x_{min})}{N_x} \quad (4)$$

$$\Delta_y = \frac{(y_{max-}y_{min})}{N_y} \quad (5)$$

$$\Delta_z = \frac{(z_{max-}z_{min})}{N_z} \quad (6)$$

According to [36], the dense point cloud (P) was defined as an unordered collection of n points $\{P_i\}_{i=1}^{n}$ in 3D Euclidean space, resulting from the scanning of an object and representing the surface of that object. The columns representing the x, y and z axes of this dense point cloud P_x , P_y and P_z were divided by their corresponding actual voxel dimension and rounded using the round function shown in (7), (8) and (9). Dim_x, Dim_y, and Dim_z were then horizontally concatenated and composed the rounded point cloud Dim, as in (10). This was effectively a dimensionless array that indicated which voxel grid each point belonged to with an integer index for axes x, y and z. As there were multiple points for each voxel, the recurring points were removed. This was done by finding the unique rows of the rounded point cloud Dim using the unique function. The result is the dimensionless voxelized point cloud DVC, with only one occasion of each voxel as in (11). The empty voxelized point cloud EVC, is the dimensionless voxelized point cloud multiplied by the respective voxel dimensions Δ_x, Δ_y, Δ_z, as in (12).

$$Dim_x = \text{round}(\frac{(P_x)}{\Delta_x}) \quad (7)$$

$$Dim_y = \text{round}(\frac{(P_y)}{\Delta_y}) \quad (8)$$

$$Dim_z = \text{round}(\frac{(P_z)}{\Delta_z}) \quad (9)$$

The rounded point cloud was composed of the results of (7), (8) and (9) horizontally concatenated:

$$Dim = [Dim_x, Dim_y, Dim_z] \quad (10)$$

The dimensionless voxelized point cloud was found from the following equation:

$$DVC = \text{unique}\ [Dim_x, Dim_y, Dim_z] \quad (11)$$

The empty voxelized point cloud (EVC) was equal to the dimensionless voxelized point cloud (DVC) multiplied by the corresponding actual voxel dimension as in the following equation:

$$EVC = [Dim_x \times \Delta_x, Dim_y \times \Delta_y, Dim_z \times \Delta_z] \quad (12)$$

The empty voxelized point cloud, EVC was the final product of voxelization. Essentially, this is a point cloud which describes the dense point cloud as a sum of the active voxels. With the term active voxel, one means that it is occupied by at least one point of the dense point cloud. Figure 3**Error! Reference source not found.**c shows the empty voxelized point cloud.

As previously stated, if the voxel size (or $Grid$) were smaller than the available point cloud surface density, then there would be voids where the gridline was not occupied by active points. The mean surface densities of the dense point cloud were measured to find the smallest permissible voxel size with the given dense point cloud. This was determined by measuring the population of the point clouds within an area of 1 m^2. This was done in CloudCompare with the density measure function using a circular radius of 0.564, corresponding to an area of calculation of 1 m^2. The mean surface densities of the empty voxelized point cloud and the dense point cloud were 25 and 855 points/m^2 (as shown in Figure 3**Error! Reference source not found.**a,c). Based upon experimentation with the above dense point cloud, the smallest voxel size permissible for the above dense point would be equal to 1 cm.

3.2.2 Step 4: Voxelized point cloud - void filling

This was a key step of the procedure since the geometrical domain occupied by the 3D structure was hollow and thus it was carried out by means of a multiple filling of the voxelized point cloud surfaces. Similar to [19], the voxelized point cloud was treated as a stack of raster images with common pixel size and dimension and characterized by a specific height, z. **Error! Reference source not found.**Figure 3**Error! Reference source not found.**d-e shows the raster images of the empty and filled voxelized point clouds for a horizontal section of the tower. This section was at an arbitrary height equal to 3.75 m. In specific, the active voxels are shown in white colour. To fill the whole domain, the raster image corresponding to each of the voxelized point cloud heights was morphologically opened and closed. The perimeter of the empty voxel cloud needed to be continuous, so that its' contained area may later be filled. If the perimeter of the empty voxel were not continuous, it could have been modified and closed. All the inactive pixels which were found to be contained inside the perimeter of the tower were converted into active pixels, thereby resulting in the filled voxelized point cloud. These functions can be applied to any type of point cloud. All these procedures have been fully automated and incorporated into the voxelization algorithm.

3.2.3 Step 5: Geometric model development - voxelized model

In step five, the geometric model development was carried out. For the case of the tower investigated in this study, DEM numerical modelling undertaken using the software 3DEC [37]. Each block of the geometric model was defined as an 8-noded polyhedron. The polyhedron development was based upon assigning the polyhedron nodes in clockwise order, for two parallel faces of each voxel of the cloud. This was an automatic procedure within the voxelization algorithm developed in this study. Figure 3f shows the 50 cm model which consists of 9,407 blocks.

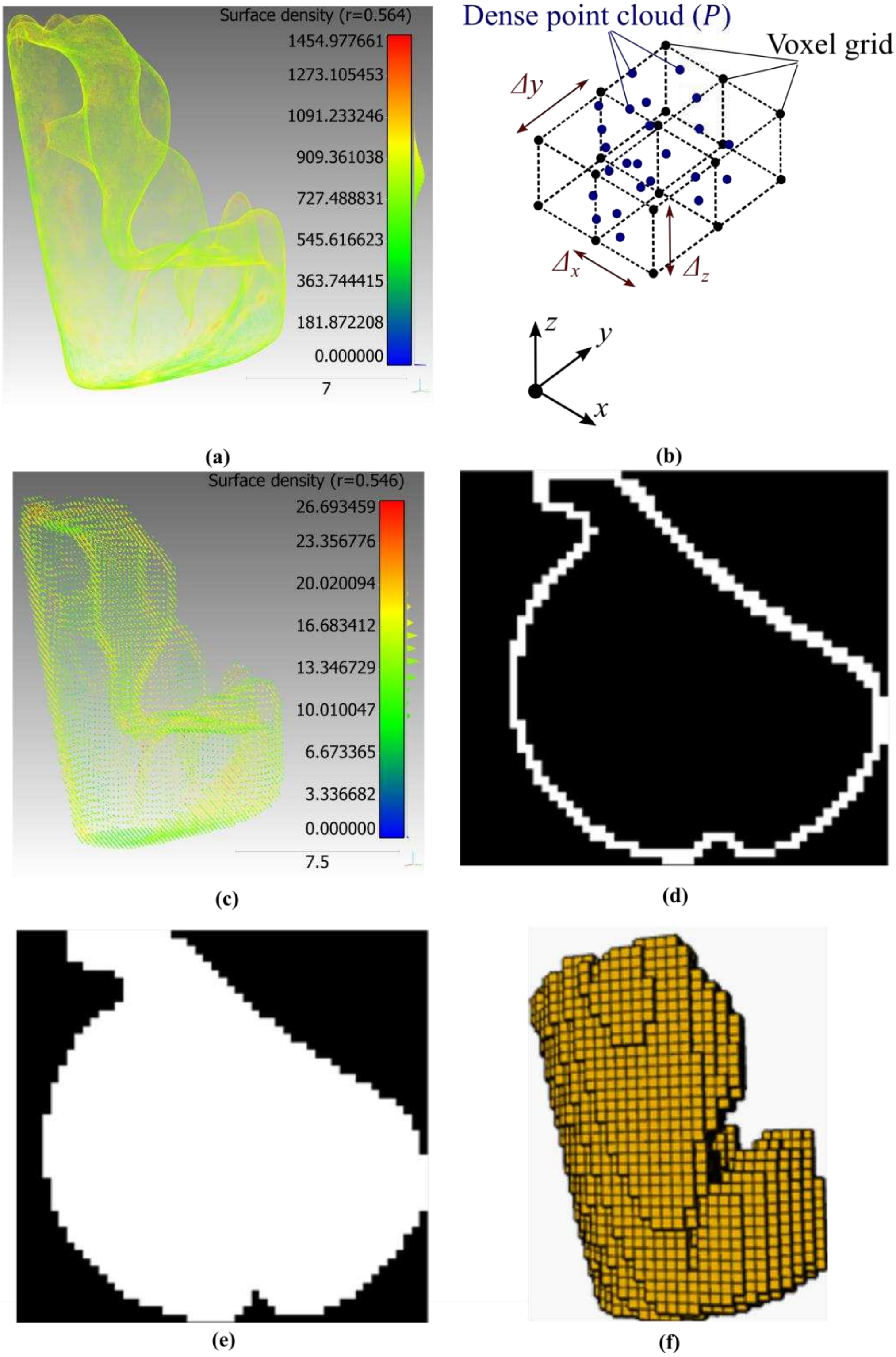

Figure 3. Voxelization: (a) dense point cloud; (b) voxelization process; (c) empty voxelized point cloud. Void filling: (d) empty; and (e) filled raster image for z equal to 3.75 m of the voxelized point cloud. Geometric model development (f)

3.2.4 Step 6: Geometrical assessment

The geometrical accuracy of the geometric models was assessed by comparing their properties with that of a reference mesh. This was a watertight mesh constructed using the Poisson Surface Reconstruction algorithm of the dense point cloud prior to voxelization (Figure 4a). For the watertight mesh generation, the octree depth was 12 (the term octrees refers to the partitioning of the 3D space by recursively sub-dividing it into eight octants-octrees which are a 3D analogy of quadtrees), samples per node were 1.5, the full depth was 5, the point weight was 4.0 and the boundary was free. The mesh was made with a plugin of CloudCompare [34] based on the well-known Poisson Reconstruction algorithm [38]. Initially, a volumetric comparison was carried out to assess the error in the volume of the geometric models. In addition, the absolute cloud-to-mesh (C2M) distances were calculated between the empty voxelized point clouds and the reference mesh (Figure 4b) to assess the surface errors of the geometric model. This was again carried out in CloudCompare. During the voxelization, there was no displacement or rotation of the point cloud involved. Thus, for comparison between the voxelized and dense point clouds, alignment was not required.

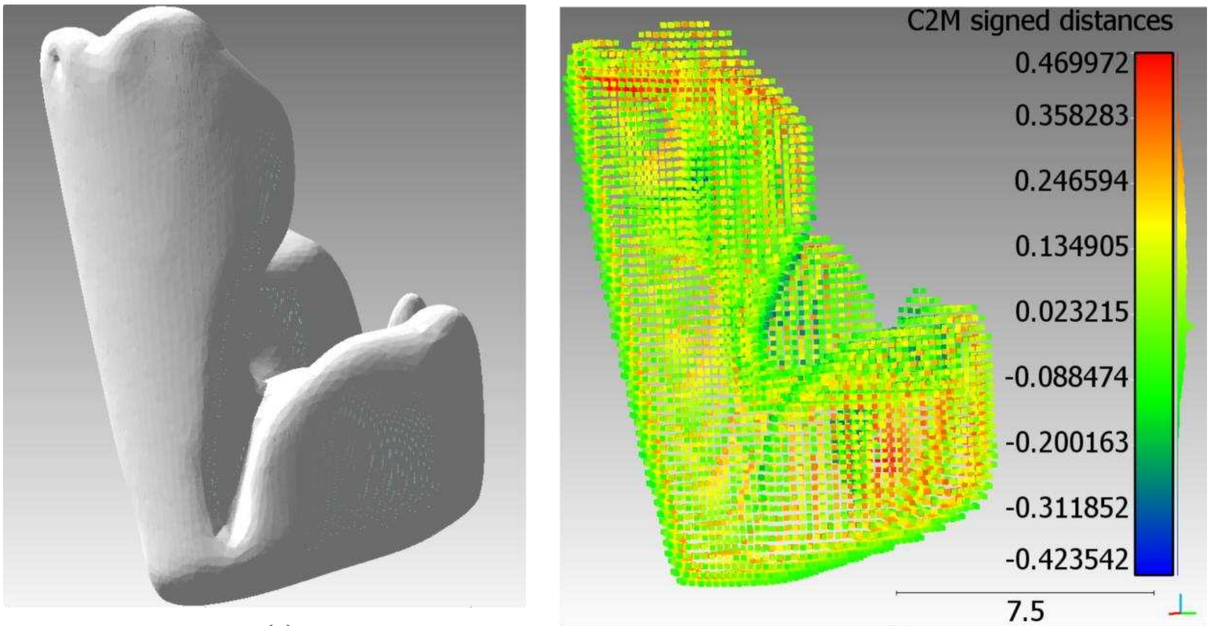

(a) (b)

Figure 4. Geometric assessment: (a) watertight mesh; and (b) cloud-to-mesh distance of the 50 cm voxelized model with the watertight mesh.

3.2.5 Step 7: Geometric model refinement - refined voxelized model

A procedure of geometric model refinement was developed to increase the volumetric accuracy of the voxelized models. This was done by using the same dimensionless point cloud of the voxelized model and an altered voxel dimension prior to geometric model development. The coefficient for adjusting the voxel dimension, termed the volume adjustment coefficient (VAC), was obtained from equation (13) below. The refined voxelized model volumes were obtained from (14).

$$VAC = \sqrt[3]{\frac{(Watertight\ mesh\ volume)}{(Voxelized\ model\ volume)}} \tag{13}$$

$$Refined\ voxelized\ model\ volume = (Voxelized\ model\ volume) \times VAC^3 \tag{14}$$

3.3 Structural analysis with the discrete element method – Stage 3

3.3.1 Step 8: Block and mortar joint definition

DEM is an approach that has been widely used to simulate the static and dynamic behaviour of blocky structures. Within DEM, masonry units (i.e. blocks) are represented as rigid or deformable blocks, which may form any arbitrary geometry. Interactions between blocks are governed by appropriate stress-displacement constitutive laws at point contacts at the edges of the blocks [37]. The motion of the blocks is simulated throughout a series of small but finite time-steps, numerically integrating the Newtonian equations of motion. Contacts in blocks can be face-to-face, vertex-to-face or edge-to-edge type. The seldom case of edge-to-edge is shown in Figure 5a. Finite displacements of the discrete bodies and rotations are allowed which includes the complete detachment of blocks and new contact generation as the calculation proceeds. Forces are considered as linear functions of the actual penetration in the shear and normal directions [1].

Figure 5b-c show the adopted Mohr-Coulomb joint constitutive model implemented in 3DEC. The in-elastic material properties used within these models were the joint cohesive strength (C), the joint tensile strength (T), and the joint friction angle (φ). According to the adopted joint constitutive model, the structure's behaviour is governed by the joint normal and shear stiffnesses, K_n and K_s in the normal and shear elastic range accordingly.

In the model, the tensile normal force is limited to T_{max} and the shear force is limited to F^s_{max} ; see equations (15) and (16); where T is joint tensile strength, A_c is the sub-contact area, C is joint cohesive strength and φ is the joint friction angle.

$$T_{max} = -T \times A_c \quad (15)$$

$$F^s_{max} = c \times A_c + F^n \times tan\,\varphi \quad (16)$$

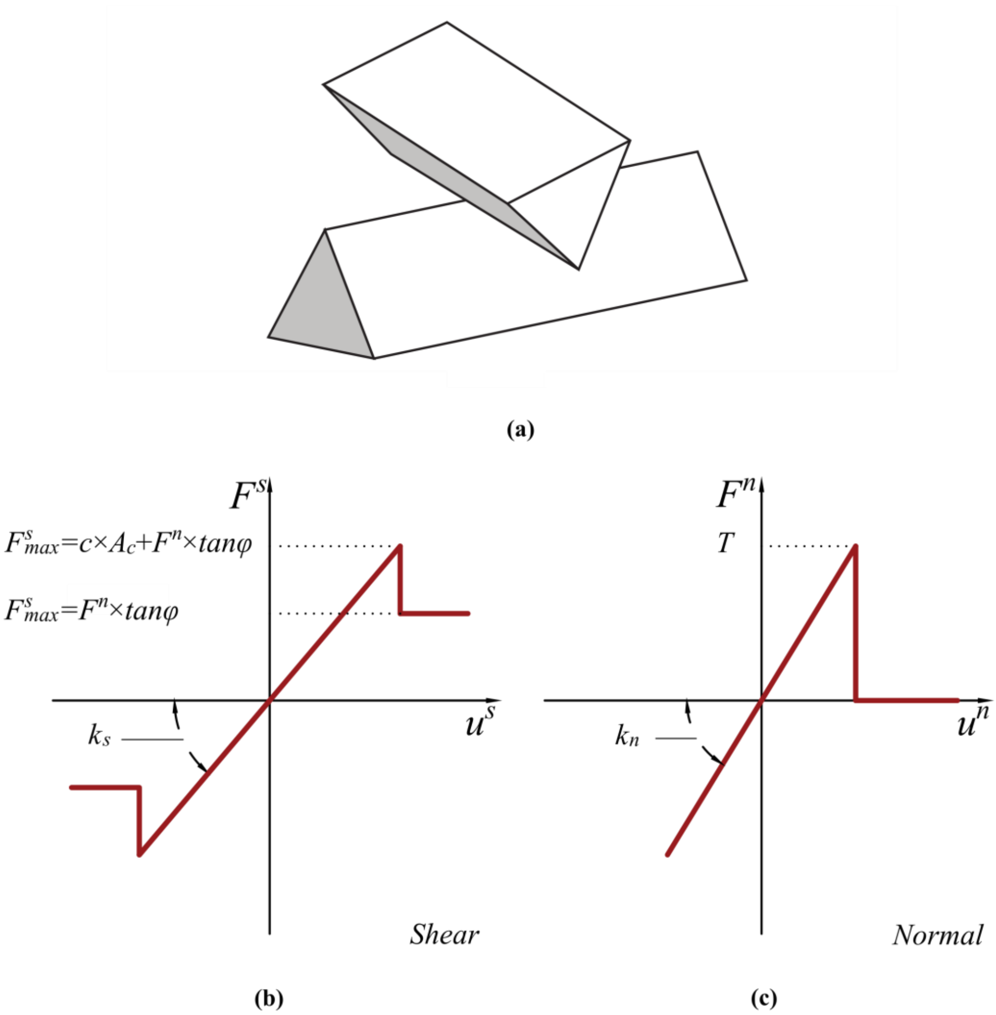

Figure 5. Contact between two blocks: the seldom edge-to-edge type contact (a) [37]. Force-displacement relationship of the adopted joint constitutive model for: (b) shear; and (c) normal direction.

3.3.2 Step 9: Selection of material properties for the DEM model

In general, when modelling periodic in texture masonry structures with DEM, the masonry units are represented as an assemblage of distinct blocks separated by zero thickness interfaces at each mortar joints. However, in this study, since we are dealing with rubble masonry, the tower was discretised into equal in shape blocks/voxels. In a rigorous way, a homogenization procedure such as the one proposed in [39] should be used to set up the material properties which characterise the mechanical interaction between blocks. However, since the present study mainly focuses on the "*point cloud to structural analysis*" framework, for simplicity, material properties were obtained from the literature. The material properties used in this study are shown in Table 1. Generally, the numerical values of the material properties used in this study satisfied at least one of the following three criteria: (a) a proximity to the actual physical properties of historic masonry structures; (b) a proximity to values previously used in numerical modelling with the same numerical method (DEM); and (c) an overall structural capacity estimation in general agreement with previous research on historic masonry structures, e.g. [21]. Blocks were modelled as rigid elements having a density equal to 1,900 kg/m^3, obtained from a previous investigation on the specific tower [21]. The joint normal (K_n) and shear (K_s) stiffnesses were taken equal to 20 and 15 GPa/m, respectively. The joint friction angle (φ) between blocks was taken as 25 degrees, while the joint tensile (T) and cohesive (C) strength at the joints were both taken equal to 0.25 MPa; to represent old and deteriorated low bond strength masonry.

Table 1. Mechanical properties of the zero-thickness interface in the numerical models.

Parameter	Symbol	Unit	Model Values
Joint Normal Stiffness	K_n	GPa/m	20
Joint Shear Stiffness	K_s	GPa/m	15
Joint Cohesive Strength	C	MPa	0.25
Joint Tensile Strength	T	MPa	0.25
Joint Friction	φ	°	25

3.3.3 Step 10: Boundary condition definition

As the base of the voxelized models resulting from the given point cloud of the tower was not flat, an additional base was generated. This was in order to define a level, planar support to the tower. This process was carried out fully automatically within the voxelization algorithm by means of extending the dimensionless point cloud in the direction of the z-axis. Figure 6a-c shows the original geometric model, the additional base and the final numerical model used for structural analysis.

After adding the base, a level plane (Πo) was defined as the boundary of fixed and free-moving blocks. This is shown in Figure 6d (at the lowest course of the blocks of the original numerical model) and defines the boundary between the fixed and free-moving blocks. Below this level, blocks were fixed against movement in all directions (the dark grey zone shown in Figure 6e), while above this level the blocks were considered to represent the rubble masonry and were free to move (the silver zone shown in Figure 6e). By adding this additional base and ensuring planar support, failure of the structure enabled by means of material degradation only, and not support failure.

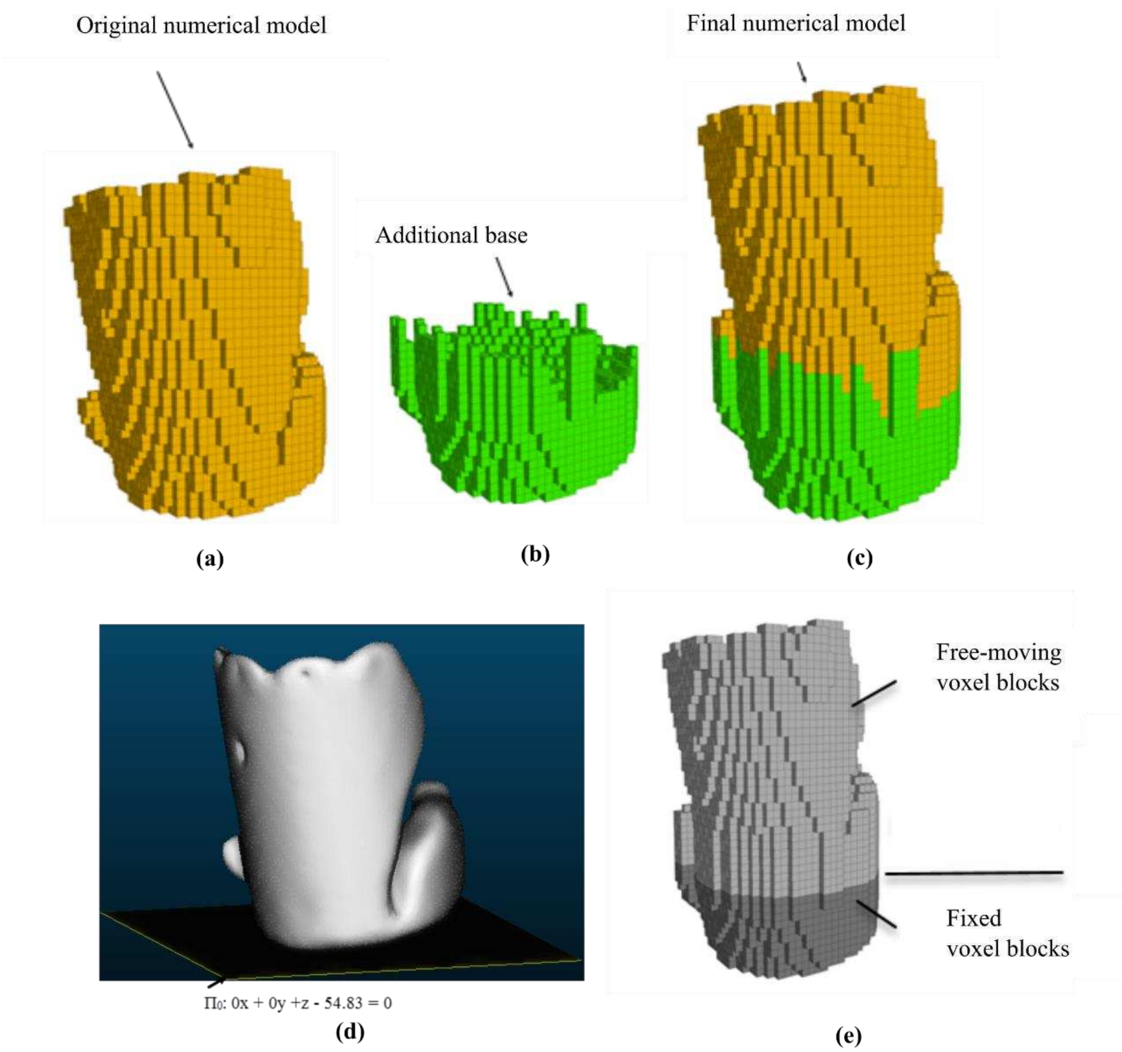

Figure 6. View of the numerical model of the tower developed using DEM: (a) original geometric model derived from point clouds; (b) base added to assist with the numerical simulations; (c) final numerical model (note that green colour refers to an additional base while gold colour relates to the original 50 cm voxelized model). Boundary conditions of tower visualized in: (d) point cloud; and (e) numerical model.

3.3.4 Step 11: Loading protocol definition

In the numerical model, a tilt plane analysis was performed with the aim of quantifying the maximum theoretical inclination angle (θ_t) of the tower, if it were situated on a tilted plane. This value was effectively the measure of the tower's structural capacity. The inclination angle was estimated by applying a horizontal acceleration (g_h) equal to $\lambda_h \times$ g, see equation (17) and altering the vertical acceleration of gravity from g to g_{vz} , equal to $\lambda_v \times$ g, see equation (18). The horizontal and vertical inclination angle multipliers λ_h and λ_v were obtained from the equations (17) and (18). Figure 7**Error! Reference source not found.**a shows a view of the tower with the gravitational acceleration components annotated.

$$\lambda_h = \sin(\theta_t) \quad (17)$$

$$\lambda_v = \cos(\theta_t) \quad (18)$$

Figure 7**Error! Reference source not found.**b shows the plan of the tower base and the azimuth (ψ) of inclination (i.e. horizontal direction in which the inclination takes place). In the numerical model, 3D loading due to the theoretical inclination was achieved by assigning gravitational acceleration components as per equations (19) to (21).

$$g_{hx} = g \cdot \lambda_h \cdot \cos\psi \quad (19)$$

$$g_{hy} = g \cdot \lambda_h \cdot \sin\psi \quad (20)$$

$$g_{vz} = g \cdot \lambda_v \quad (21)$$

In particular, equations (19), (20) and (21) describe the x-axis horizontal component, y-axis horizontal component, and vertical component of gravity, respectively (as shown in Figure 7**Error! Reference source not found.**a-b). So, for any given azimuth of inclination (ψ), the theoretical inclination angle (θ_t) is proportional to the horizontal component of gravity applied to the structure. The resulting destabilization is common with that of a tilt-table, parallel to the azimuth of inclination (ψ). The structural analysis of this investigation was carried out for an azimuth of ψ equal to 60° (Figure 7**Error! Reference source not found.**b). This was due to the structure's pre-existent inclination being most significant in this direction [21].

Starting from a value of θ_t equal to 0 (no inclination), the theoretical inclination angle θ_t was increased incrementally. During the simulation, the inclination angle multiplier λ_h (corresponding to θ_t) was recorded. The critical inclination angle $\lambda_{h,max}$ was employed to assess the load-bearing capacity of the structure, equal to the inclination angle multiplier at which the structure could not arrive at equilibrium at the end of a given loading cycle. This was calculated by monitoring both the total unbalanced force of the model and the so-called inclination angle multiplier-displacement curves of strategically selected monitored points. The unbalanced force [37] in specific is a metric employed to evaluate the mechanical equilibrium state of the model (and subsequent occurrence of the joint slip or plastic flow), during structural analysis. Equilibrium of the model is achieved when either the net nodal force vectors at each block centroid or gridpoint are equal to zero and this is monitored in form of: a) the maximum nodal force vector termed the "unbalanced" or "out-of-balance" force; or alternatively b) the ratio of the unbalanced force towards the representative forces of the system, termed "unbalanced force ratio". During the structural analysis of this investigation, an unbalanced force ratio equal to 1e-4 was employed. This means that during the loading, increments were added as long as the unbalanced force ratio was smaller to or equal to 1e-4. The monitored points at Points A, B and C, shown in Figure 7**Error! Reference source not found.**c were strategically selected, being situated: a) on the azimuth of theoretical rotation of ψ equal to 60 °; and b) at various heights (top, mid-height and bottom). This selection of the monitored points ensured reliable information about the structure's behaviour was provided for global and local failure, in the principal direction of loading. It's noteworthy that further than the critical inclination angle multiplier $\lambda_{h,max}$, the critical horizontal displacements $U^A_{h,max}$, $U^B_{h,max}$ and $U^C_{h,max}$ of the monitored points A, B and C were employed as a metric of quantifying the tower's deformation capacity.

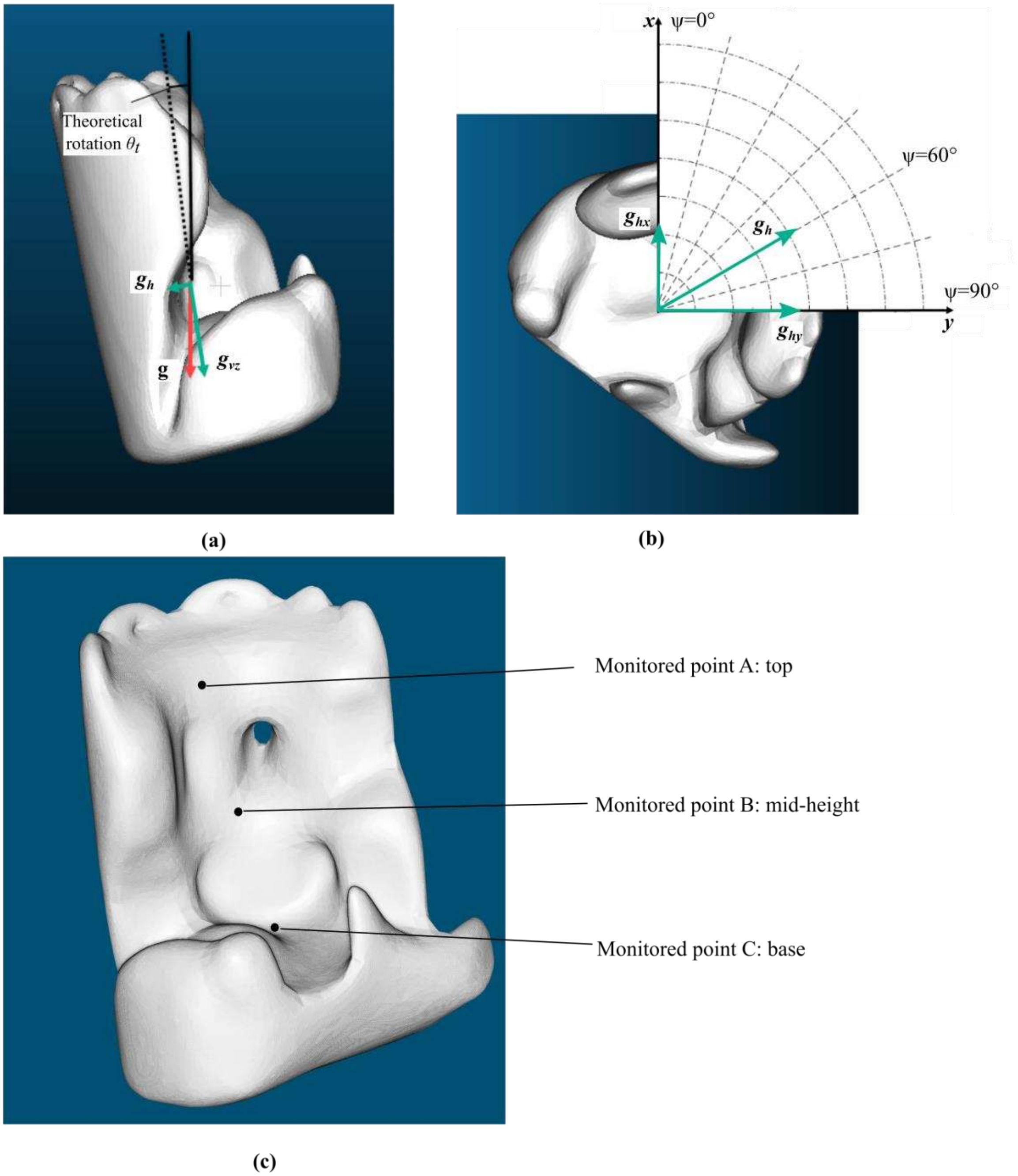

Figure 7. The tower with gravitational acceleration components annotated (the green vertices denote the gravitational acceleration components for a theoretical inclination angle of θ_t): (a) view; and (b) plan of the tower base with the azimuth of inclination (ψ). Monitored points A, B and C at the top, mid-height and base of the tower (c).

3.3.5 Step 12: Partitioning strategy (optional)

In the case that the numerical model was either non-executable or computationally unmanageable due to the number of contacts, then a partitioning strategy should be adopted. Historic masonry structures are characterised by low bond strength and failure due to shear at the mortar joints or by hinge formation. In specific, the formation of the hinges in the tower allows the rotation of some of the blocks while restricting the rotation of others. In this case, we can have areas of high strength concentration Displacements due to external load applied to the tower are accompanied by the opening and shear sliding of the blocks. As inclination angle increases in the tower, hinges are formed as bricks slide and rotate against each other. According to Mifsud [40], the development of hinge formation depends on the material properties of masonry, the geometric characteristics and confinement of blocks as well as the load distribution in the structure. This effectively means that partitions of structure that are not prone to failure can be considered rigid. In the numerical model, such partitions were defined by joining the elements that were desired to form rigid bodies in the structural analysis model. This strategy requires that the analyst has *a priori* knowledge to where the hinge formation is most likely to occur, the herein termed failure zone of the structure.

The employment of partition strategy is particularly advantageous in terms of optimization of computational resources and increasing geometrical accuracy. Since the number of free-moving blocks of the calculation cycle is reduced, computational resources are optimized for a given voxel size. Furthermore, as will be demonstrated in the forthcoming paragraphs, voxel size reduction significantly increases block numbers yet also increases geometrical accuracy. Thus, owing to the optimization of computational resources, numerical models can be executed with a larger number of voxels (of a decreased voxel size) with improved geometrical accuracy.

4 Application of the proposed framework in the case study

Various geometric models of the Caerphilly tower with different voxel sizes have been developed. Figure 8 shows three numerical models with a voxel size equal to 50, 40 and 30 cm. Though another three models with a voxel size of 25, 20 and 10 cm were also developed, structural analysis was not undertaken since they were found to be computationally unmanageable with the available computational resources. This inability to simulate smaller voxel size models was a result of the unmanageable number of free-moving blocks and total contacts. As will be demonstrated further on, the best compromise between structural capacity estimation, geometric accuracy and computational time was represented with the 30 cm voxel size. Thus, for the voxel size of 30 cm, the sensitivity of the voxel orientation was also investigated on the structural capacity.

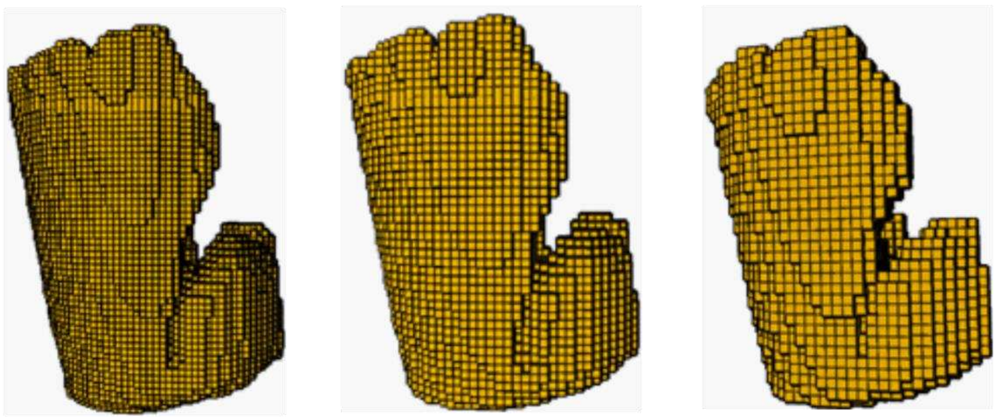

Figure 8. Voxelized models of the tower developed using different voxel sizes: (a) 30 cm; (b) 40 cm; (c) 50 cm

4.1 Influence of the voxel size on the characteristics and structural capacity of the tower

Error! Reference source not found. Table 2 shows the characteristics of the developed voxelized models, including: a) geometric accuracy (volumetric differences and cloud-to-mesh distances); and b) geometric model characteristics (block and contact numbers). From Table 2**Error! Reference source not found.**, the volumetric error exponentially decreases as the voxel size in the model decreases. Also, for voxel sizes below and equal to 25 cm (that correspond to an error of equal to 5.3 %), voxelized models without refinement could be considered acceptable; all voxel sizes above 25 cm needed numerical model refinement. The difference in mean cloud-to-mesh distance of the voxelized models and refined voxelized models shows that the model refinement can induce error to the external surfaces of the structure. Concerning the geometric model properties and computational times, all the quantities were inversely and exponentially proportional to the voxel size. From Table 2**Error! Reference source not found.**, it also appears that the larger the size of the voxel, the faster the numerical simulation is. Furthermore, the best compromise between structural capacity estimation, geometric accuracy and computational time was represented with the 30 cm voxel size. Considering simulation times with the available resources (i.e. an Intel(R) Xeon(R) CPU @ 3.00 GHz processor and 64 GB memory RAM), a model containing 40,000 free-moving blocks and 240,000 total contacts (voxel size of 30 cm) was developed and adopted in this study

Table 2. Characteristics of the voxelized models.

	Voxel size (cm)	Geometrical accuracy					Geometric model properties	
		VAC	Volume (m^3)	Volume error %	Mean C2M (cm)	St. dev. C2M (cm)	Blocks	Total Contacts
Voxelized models	50 cm	1	1028	19.5	0.1	20.4	13,385	155,556
	40 cm	1	980	13.9	0	16.4	22,532	266,296
	30 cm	1	933	8.5	0.1	12.1	47,827	576,449
	25 cm	1	911	5.9	0.2	10.1	74,969	912,491
	20 cm	1	886	3.0	0.1	8	111,821	2,552,214
	10 cm	1	836	-2.8	0	3.7	844,343	10,645,763
Refined Voxelized	50 cm	0.943	862	0.2	8.2	27.3	13,385	155,556
	40 cm	0.958	862	0.2	11.5	20.6	22,532	266,296
	30 cm	0.974	862	0.2	9	13.9	47,827	576,449
	25 cm	0.981	860	0.0	6.2	11.2	74,969	912,491
	20 cm	0.990	859	-0.1	3.3	8.4	111,821	2,552,214
	10 cm	1.009	859	-0.2	3.5	4.8	844,343	10,645,763

For the voxel sizes of 50, 40 and 30 cm, the influence of the voxel size upon the structures' load-bearing capacity, deformation capacity and failure mode was investigated. Table 3 reports the results of the structural analysis of the 50, 40 and 30 cm voxelized models for an azimuth of inclination (ψ) equal to 60°. From Table 3, its evident that the decrease of voxel size is associated with: a) decrease in load-bearing capacity (i.e. the critical inclination angle multiplier); b) decrease in the deformation capacity (i.e. the critical horizontal displacements of monitored points A, B and C). This is in agreement with a previous investigation on the out-of-plane loading of masonry structures with the DEM [41], that block size significantly influences the structural capacity. The reasoning behind this that effectively, the joints form planes of weakness in the structure. As the voxel size decreases, the number of joints significantly increases, resulting in a consequent reduction of the structural capacity. It is hypothesized that this reduction would become negligible for a voxel size lower than a certain threshold, yet this should be examined in further investigation.

Further than results of Table 3, the accompanying failure modes and inclination angle multiplier-displacement curves are shown in Figure 9a-b, Figure 9c-d and Figure 9e-f respectively. It's noteworthy that the blue, green and red cuboids located on the joints signify joint tensile failure, current joint slipping and past slipping respectively. Furthermore, the displacement contours of the blocks are plotted demonstrating the magnitude of displacement due to inclination. From Figure 9a, c, e, it's evident that failure modes of the models were common and consisted of perimetrical cracks developed at the junction of the remaining up-right body and base of the tower progressing towards the base. With the application of any further inclination, the remaining up-right body detached and began to rotate freely (simultaneously breaking up into pieces. Similar failure modes were observed in a previous study [21].

Table 3. Influence of voxel size on structural capacity.

Voxel size (cm)	$\lambda_{h,max}$	$U^{A}_{h,max}$ (mm)	$U^{B}_{h,max}$ (mm)	$U^{C}_{h,max}$ (mm)
50 cm	0.18	6	3.8	1.8
40 cm	0.14	5.6	3.0	1.4
30 cm	0.06	2.0	1.0	0.3

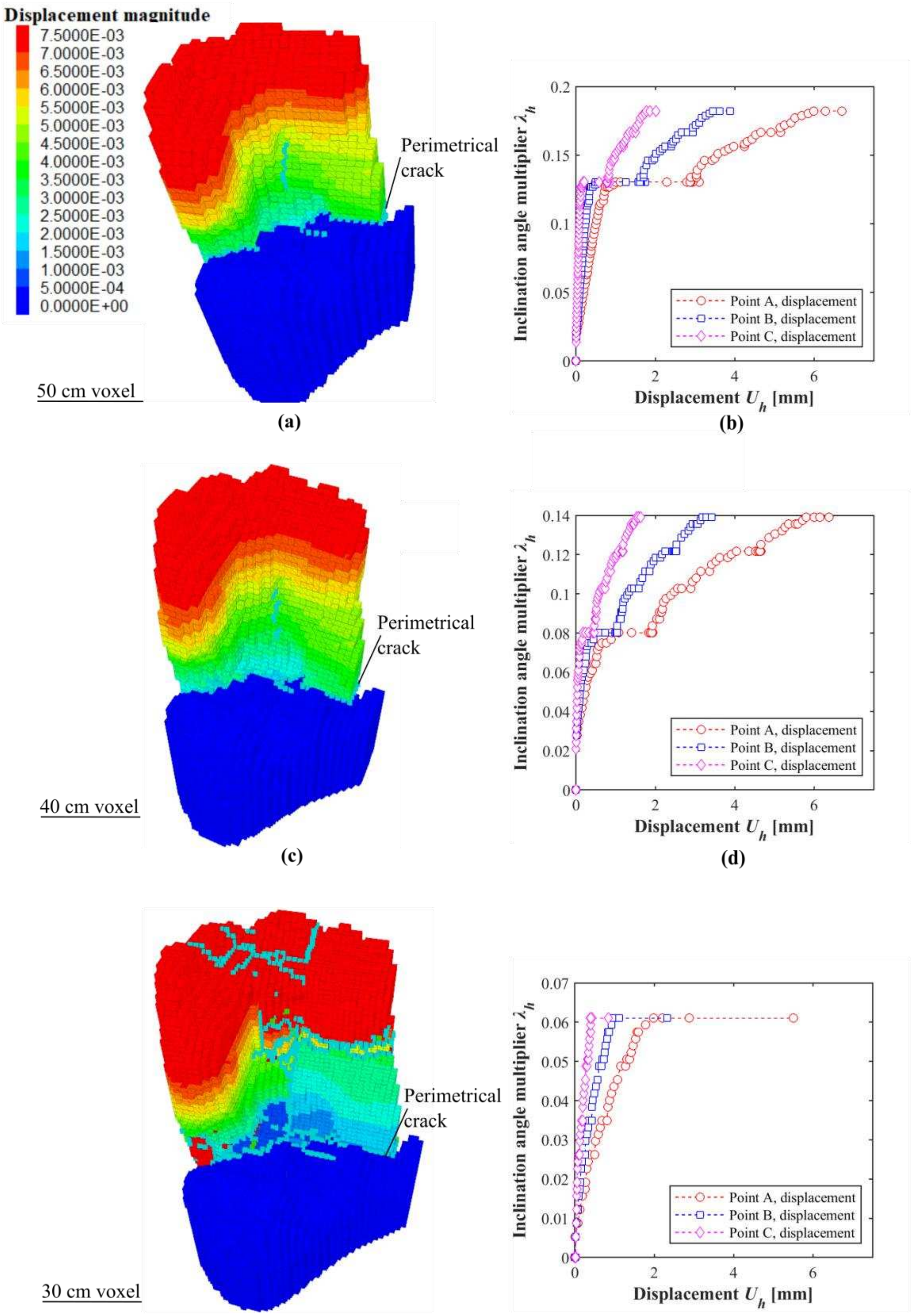

Figure 9. Failure modes and inclination angle multiplier-displacement curves (different scale) of: (a-b) 50 cm; (c-d) 40 cm (e-f) 30 cm voxel size models (azimuth of inclination ψ equal to 60°). The blue markers denote joint tensile failure while the displacement contour is common and in meters.

4.2 Influence of the voxel orientation on the structural capacity of the tower

For the voxel size of 30 cm, the influence of the voxel orientation upon the structures' load-bearing capacity, deformation capacity and failure mode was investigated. With respect to Figure 9**Error! Reference source not found.**, the horizontal voxel principal directions were altered by rotation of the dense point cloud, prior to voxelization. Two simulations were performed whereby the dense point cloud was rotated by 30 and 60 degrees prior to voxelization around the z-axis and loaded for ψ equal to 60°.

Table 4 reports the results of the structural analysis of the models with a voxel rotation. From Table 4, it's evident that, in comparison with the original 30 cm voxel size model of Table 3, the models with a voxel rotation demonstrated: a) comparable load-bearing capacities (i.e. the critical inclination angle multiplier); and b) comparable deformation capacities (i.e. the critical horizontal displacements of monitored points A, B and C). Furthermore, the failure modes and inclination angle multiplier-displacement curves of the models with the voxel rotation are shown in Figure 10a-b and Figure 10c-d respectively. Comparing the differences between Figure 9e-f and Figure 10**Error! Reference source not found.**, it is evident that the failure modes and inclination angle multiplier-displacements curves between the models with voxel rotation and original 30 cm voxel size model show a good agreement.

Table 4. Influence of voxel orientation on structural capacity.

Voxel rotation	$\lambda_{h,max}$	$U^A_{h,max}$ (mm)	$U^B_{h,max}$ (mm)	$U^C_{h,max}$ (mm)
30°	0.06	2.0	1.0	0.4
60°	0.08	2.4	1.0	0.4

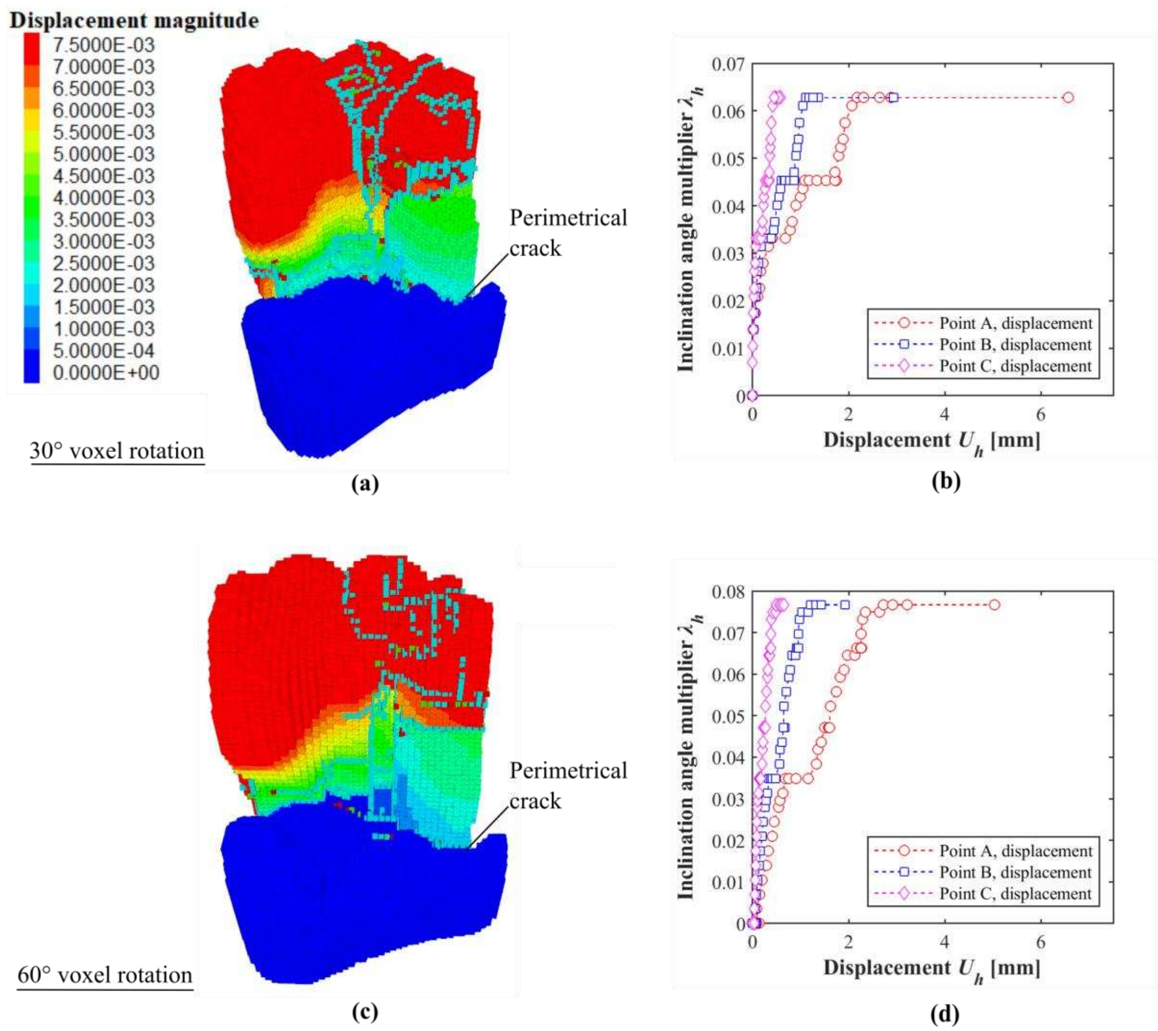

Figure 10. Failure modes and inclination angle multiplier-displacement curves of 30 cm voxel size with: (a-b) 30° voxel rotation; and (c-d) 60° voxel rotation. The blue markers denote joint tensile failure while the displacement contours are common and in meters.

5 Conclusions

Predicting the mechanical behaviour of rubble masonry structures is a complex task due to their highly nonlinear behaviour. Numerical methods such as the DEM have been demonstrated as highly effective for accurately capturing the in-service, collapse and post-collapse behaviour of masonry structures. Due to its numerical formulation which was specifically developed for rock mechanics (i.e. specific problem of sliding of rocks), the DEM permits the discrete and non-linear behaviour of the tower to be better represented than other numerical methods such as the FEM, yet it requires detailed metrical geometric information of the structure subject to structural analysis. So far, the geometry of rubble masonry structures is captured with traditional geospatial techniques (e.g. visual inspection and CAD-based design methods) which are labour intensive and error-prone. Over the last 10 years, advances in terrestrial laser scanning and SfM photogrammetry have drastically changed the building industry since such techniques are able to rapidly and remotely capture millions of points of the entire scene, resulting in point clouds. This paper presents a novel framework for the expeditious and automatic modelling of rubble masonry, directly from a dense point cloud, and without the need for mesh development. The proposed "point cloud to structural analysis" framework consists of three stages and nine steps. The three-stage framework involved: Stage 1 - 3D documentation; Stage 2 - geometric model development; and Stage 3 -structural analysis. The methodological workflow proposed here has been demonstrated on the southwest leaning tower in Caerphilly castle. A quantitative structural assessment of the specific rubble masonry tower undertaken. The geometry of the tower was represented by the sum of hexahedral blocks (voxels) defined by the user. The main findings of this investigation are summarized below:

- The potential of the proposed "point cloud to structural analysis" framework has been demonstrated to quantitatively assess the three-dimensional mechanical behaviour of complex in geometry rubble masonry structures such as towers.
- As the voxel size decreases, the load-bearing and deformation capacity decreases. This is in agreement with a previous investigation on the out-of-plane loading of masonry structures with the DEM [41]. Furthermore, due to voxel size decrease, the computational time required to perform structural analysis increases dramatically and could lead to models that cannot be handled with standard workstations.
- For the case study investigated herein (i.e. the Caerphilly tower), for a course voxel size of 50 cm, structural analysis was carried out in a manageable computational time of 71 minutes for a geometric model with 9,000 blocks, 100,000 contacts.
- Finally, the best compromise between, geometric accuracy and computational time was achieved with a voxel size of 30 cm. This was very close to the size of the masonry stones observed on the structure. However, such model resulted in a less manageable computational time of approximately 238 minutes.

The above findings suggest that with the proposed procedure, it is possible to perform unprecedented structural analyses of rubble masonry structures with high-level structural analysis methods such as the DEM in a manageable time. This contribution paves the way for their automated structural analysis of large, complex in geometry and discontinuous in nature masonry structures.

To increase the reliability of the structural analysis of the proposed approach, further investigation would be beneficial on the effect of the mechanical properties of the interface, the size of the block and orientation of the blocks, and computation resource optimization techniques. Furthermore, since rubble masonry possesses voids and flaws, a future investigation should also be carried out to simulate this by removing voxels in critical locations. Finally, due to the orthogonal nature of the voxels, analysing curve forms, such as domes, arches, can be cumbersome leading to problems such as shear-locking that does not permit, hinging failure mechanism. The overcome this, the development of automated approaches employing non-orthogonal blocks such as those in [42,43] is suggested.

Acknowledgements

The work presented in this paper has been financially supported by an EPSRC doctoral training award (case/179/65/82). The authors also gratefully acknowledge Dr Oriel Priezman for providing the point cloud of the southwest tower of Caerphilly Castle.

References

[1] J.V. Lemos, Discrete element modeling of masonry structures, International Journal of Architectural Heritage 1 (2) (2007), pp. 190-213, DOI: 10.1080/15583050601176868
[2] V. Sarhosis, J.V. Lemos, A detailed micro-modelling approach for the structural analysis of masonry assemblages, Computers & Structures 206 (2018), pp. 66-81, DOI: 10.1016/j.compstruc.2018.06.003
[3] V. Sarhosis, K. Bagi, A.R. Lemos, G. Milani, Computational modeling of masonry structures using the discrete element method, IGI Global, Hershey, PA, USA, 2016. ISBN: 978-1-5225-0231-9
[4] J. McInerney, M.J. DeJong, Discrete element modeling of groin vault displacement capacity, International Journal of Architectural Heritage 9 (8) (2015), pp. 1037-1049, DOI: 10.1080/15583058.2014.923953
[5] P. Meriggi, G. de Felice, S. De Santis, F. Gobbin, A. Mordanova, B. Pantò, Distinct element modelling of masonry walls under out-of-plane seismic loading, International Journal of Architectural Heritage 13 (7) (2019), pp. 1110-1123, DOI: 10.1080/15583058.2019.1615152

[6] B. Pulatsu, E. Erdogmus, E.M. Bretas, P.B. Lourenço, In-plane static response of dry-joint masonry arch-pier structures, Architectural Engineering Conference 2019, Tysons, Virginia, 2019, pp. 240-248, DOI: 10.1061/9780784482261.028
[7] E. Erdogmus, B. Pulatsu, A. Gaggioli, M. Hoff, Reverse engineering a fully collapsed ancient roman temple through geoarchaeology and DEM, International Journal of Architectural Heritage (2020), pp. 1-21, DOI: 10.1080/15583058.2020.1728593
[8] A. Mordanova, G. de Felice, Seismic assessment of archaeological heritage using discrete element method, International Journal of Architectural Heritage 14 (3) (2020), pp. 345-357, DOI: 10.1080/15583058.2018.1543482
[9] G. de Felice, Out-of-plane seismic capacity of masonry depending on wall section morphology International Journal of Architectural Heritage 5 (4-5) (2011), pp. 466-482, DOI: 10.1080/15583058.2010.530339
[10] N. Shrive, Discrete element modeling of stone masonry walls with varying core conditions: Prince of Wales fort case study, International Journal of Architectural Heritage 9 (5) (2015), pp. 564-580, DOI: 10.1080/15583058.2013.819135
[11] B. Pulatsu, E. Bretas, P. Lourenco, Discrete element modeling of masonry structures: Validation and application, Earthquakes and Structures 11 (2016), pp. 563-582, DOI: 10.12989/eas.2016.11.4.563
[12] J. Mills, D. Barber, Geomatics techniques for structural surveying, Journal of surveying engineering 57 (2004), pp. 56-64 DOI: 10.1061/(ASCE)0733-9453(2004)130:2(56)
[13] B. Riveiro, P. Morer, P. Arias, I. de Arteaga, Terrestrial laser scanning and limit analysis of masonry arch bridges, Construction and Building Materials 25 (4) (2011), pp. 1726-1735, DOI: 10.1016/j.conbuildmat.2010.11.094
[14] I. Lubowiecka, P. Arias, B. Riveiro, M. Solla, Multidisciplinary approach to the assessment of historic structures based on the case of a masonry bridge in Galicia (Spain), Computers & Structures 89 (2011), pp. 1615-1627, DOI: 10.1016/j.compstruc.2011.04.016
[15] B. Riveiro, M. Dejong, B. Conde, Automated processing of large point clouds for structural health monitoring of masonry arch bridges, Automation in Construction 72 (2016), pp. 258-268, DOI: 10.1016/j.autcon.2016.02.009
[16] B. Conde, L. F. Ramos, D. Oliveira, B. Riveiro, M. Solla, Structural assessment of masonry arch bridges by combination of non-destructive testing techniques and three-dimensional numerical modelling: Application to Vilanova bridge, Engineering Structures 148 (2017), pp. 621-638, DOI: 10.1016/j.engstruct.2017.07.011
[17] L. Truong-Hong, D. Laefer, T. Hinks, H. Carr, Combining an angle criterion with voxelization and the flying voxel method in reconstructing building models from lidar data, Computer-Aided Civil and Infrastructure Engineering 28 (2013), pp. 112-129, DOI: 10.1111/j.1467-8667.2012.00761.x
[18] L. Truong-Hong, D.F. Laefer, Octree-based, automatic building façade generation from LiDAR data, Computer-Aided Design 53 (2014), pp. 46-61, DOI: 10.1016/j.cad.2014.03.001
[19] G. Castellazzi, M.A. Altri, G. Bitelli, I. Selvaggi, A. Lambertini, From laser scanning to finite element analysis of complex buildings by using a semi-automatic procedure, Sensors 15 (8) (2015), pp. 18360–18380, DOI: 10.3390/s150818360
[20] G. Castellazzi, A.M. D'Altri, S. de Miranda, F. Ubertini, An innovative numerical modeling strategy for the structural analysis of historical monumental buildings, Engineering Structures 132 (2017), pp. 229-248, DOI: 10.1016/j.engstruct.2016.11.032
[21] A. D'Altri, G. Milani, S. Miranda, G. Castellazzi, V. Sarhosis, Stability analysis of leaning historic masonry structures, Automation in Construction 92 (2018), pp. 199–213, DOI: 10.1016/j.autcon.2018.04.003
[22] U. Almac, I.P. Pekmezci, M.G. Ahunbay, Numerical analysis of historic structural elements using 3d point cloud data, The Open Construction and Building Technology Journal 10(Suppl 2: M5) (2016), pp. 233-245, DOI: 10.2174/1874836801610010233
[23] S.M. Iman Zolanvari, D.F. Laefer, Slicing method for curved façade and window extraction from point clouds, ISPRS Journal of Photogrammetry and Remote Sensing 119 (2016), pp. 334-346, DOI: 10.1016/j.isprsjprs.2016.06.011

[24] F. Zvietcovich, B. Castaneda, R. Perucchio, 3D solid model updating of complex ancient monumental structures based on local geometrical meshes, Digital Applications in Archaeology and Cultural Heritage 2 (1) (2015), pp. 12-27, DOI: 10.1016/j.daach.2015.02.001

[25] S.G. Barsanti, G. Guidi, A new methodology for the structural analysis of 3D digitized cultural heritage through FEA, IOP Conference Series: Materials Science and Engineering, Vol. 364, Florence, Italy, 2018, pp. 1-8, DOI: 10.1088/1757-899X/364/1/012005

[26] O.E.C. Prizeman, V. Sarhosis, A.M. D'Alri, C.J. Whitman, G. Muratore, Modelling from the past: The leaning southwest tower of caerphilly castle 1539-2015, ISPRS Annals of Photogrammetry, Remote Sensing and Spatial Information Sciences, Vol. IV-2/W2, Ottawa, Canada, 2017, pp. 221-227, DOI: 10.5194/isprs-annals-IV-2-W2-221-2017

[27] D. Renn, Caerphilly Castle, Cardiff, UK: Cadw, 2002. ISBN: 978-1-85760-082-7.

[28] M. Marchi, R. Butterfield, G. Gottardi, R. Lancellotta, Stability and strength analysis of leaning towers, Géotechnique 61 (12) (2011), pp. 1069-1079, DOI: 10.1680/geot.9.P.054

[29] E.C. Hambly, Soil buckling and the leaning instability of tall structures, The Structural Engineer 63 (1985), pp. 77-85. URL: https://www.istructe.org/sitefiles/handlers/DownloadFile.ashx?productId=8009 [Accessed 19th January 2020]

[30] D. Abruzzese, L. Miccoli, J. Yuan, Mechanical behavior of leaning masonry Huzhu Pagoda, Journal of Cultural Heritage 10 (2009), pp. 480-486, DOI: 10.1016/j.culher.2009.02.004

[31] G. Milani, R. Shehu, M. Valente, Role of inclination in the seismic vulnerability of bell towers: FE models and simplified approaches, Bulletin of Earthquake Engineering 15 (4) (2017), pp. 1707-1737, DOI: 10.1007/s10518-016-0043-0

[32] J. Heyman, Leaning towers, Meccanica 27 (3) (1992), pp. 153-159, DOI: 10.1007/BF00430041

[33] M. Dejong, Seismic assessment strategies for masonry structures, Ph.D. Thesis, Department of Architecture, Massachusetts Institute of Technology, 2009. URL: https://dspace.mit.edu/handle/1721.1/49538 [Accessed 19th January 2020]

[34] CloudCompare (version 2.1), GPL software, 2019. URL: http://www.cloudcompare.org/ [Accessed 19th January 2020]

[35] T. Hinks, H. Carr, L. Truong-Hong, D. Laefer, Point cloud data conversion into solid models via point-based voxelization, The Structural Engineer 139 (2012), pp. 72-83, DOI: 10.1061/(ASCE)SU.1943-5428.0000097

[36] T. Volodine, Point cloud processing using linear algebra and graph theory, Ph.D. Thesis, Department of Computer Science, K.U.Leuven, Celestijnenlaan 200A, B-3001 Leuven, Belgium, 2007. URL: http://www.cs.kuleuven.be/publicaties/doctoraten/tw/TW2007_05.pdf [Accessed 19th January 2020]

[37] ITASCA. 3DEC 5.2 – Universal distinct element code manual. Theory and background. Mineapolis., 2019. URL: www.itasca.com [Accessed 19th January 2020]

[38] M. Kazhdan, H. Hoppe, Screened poisson surface reconstruction, ACM transactions on graphics 32 (3) (2013), pp. 1-13, DOI: 10.1145/2487228.2487237

[39] S. Casolo, Modelling in-plane micro-structure of masonry walls by rigid elements, International Journal of Solids and Structures 41 (2004), pp. 3625-3641, DOI: 10.1016/j.ijsolstr.2004.02.002

[40] J. Mifsud, Load paths in masonry construction, Phd thesis, Department of Civil & Structural Engineering, University of Malta, 2003. URL: [Accessed 19th January 2020]

[41] M. Godio, I. Stefanou, K. Sab, Effects of the dilatancy of joints and of the size of the building blocks on the mechanical behavior of masonry structures, Meccanica 53 (7) (2018), pp. 1629-1643, DOI: 10.1007/s11012-017-0688-z

[42] B. Pulatsu, E. Erdogmus, P.B. Lourenco, R. Quey, Simulation of uniaxial tensile behavior of quasi-brittle materials using softening contact models in DEM, International Journal of Fracture 217 (1-2) (2019), pp. 105-125, DOI: 10.1007/s10704-019-00373-x

[43] V. Sarhosis, T. Forgács, J.V. Lemos, Modelling backfill in masonry arch bridges: A DEM approach, in: A. Arêde, C. Costa (Eds.), 9th International Conference on Arch Bridges, Springer International Publishing, Cham, Switzerland, 2020, pp. 178-184, DOI: 10.1007/978-3-030-29227-0_16